

Article

Analysis of the Joint Bearing Capacity of Composite Cushion-Spiral Case Structures for Hydropower Stations Considering the Damage Mechanisms of Surrounding Concrete

Wenjie Xu, Gang Wang *, Zhenyue Ma and Fei Kang

School of Infrastructure Engineering, Dalian University of Technology, Dalian 116024, China; hxsuwenjie@163.com (W.X.); dmzy@dlut.edu.cn (Z.M.); kangfei@dlut.edu.cn (F.K.)

* Correspondence: gwang@dlut.edu.cn

Abstract: The spiral case structure is an essential part of a hydropower station. To accurately explore the joint load-bearing effect of the cushion-spiral case structure, a cushion-spiral case structure with a high HD value was selected, modeled, and analyzed in this study. The reliability of the model was verified through measured data. Given the contact relation between the spiral case and the cushion, the cushion laying range was used as the control parameter to investigate its impact on the joint bearing capacity of the structure. In addition, the concrete damage theory was introduced to probe the damage mechanism of the structure under assumed extreme working conditions. The steel spiral case bears most of the internal water pressure in the joint bearing system, and the bearing ratio of the surrounding concrete and reinforcement decreases with the increase in the cushion wrap angle. A 1.1–1.2 overload head is the main section that forms penetrating cracks. For the spiral case structure with a high HD value, a reasonable cushion can significantly reduce the damage level of the surrounding concrete and regulate the uneven lifting of the turbine pier and the shear strength of the stay ring. This study can provide reference points for the spiral case arrangement and range and the structural failure response under extreme working conditions.



Citation: Xu, W.; Wang, G.; Ma, Z.; Kang, F. Analysis of the Joint Bearing Capacity of Composite Cushion-Spiral Case Structures for Hydropower Stations Considering the Damage Mechanisms of Surrounding Concrete. *Water* **2024**, *16*, 112.

<https://doi.org/10.3390/w16010112>

Academic Editors: Mohammadreza Mohammadi, Moona Mohammadi and Nigel Wright

Received: 19 November 2023

Revised: 22 December 2023

Accepted: 25 December 2023

Published: 27 December 2023



Copyright: © 2023 by the authors. Licensee MDPI, Basel, Switzerland. This article is an open access article distributed under the terms and conditions of the Creative Commons Attribution (CC BY) license (<https://creativecommons.org/licenses/by/4.0/>).

Keywords: cushion-spiral case; joint bearing capacity; CDP; damage mechanism

1. Introduction

With the increasing prevalence of environmental concerns, carbon neutrality has emerged as a goal for numerous countries worldwide. Hydropower has attracted much attention as a green and pollution-free energy source [1]. Hydropower stations combine hydropower with the demand for variable resources, creating opportunities for the innovative hydropower concept [2,3]. As one of the main structures of a hydropower station, the spiral case structure (SCS) is composed of steel spiral case tubes, stay rings, and surrounding concrete, and it plays a key role in the safe and stable operation of a hydropower station due to its complex spatial and material properties [4]. The steel spiral case, cushion, and surrounding reinforced concrete may deform or crack under load. The distribution of the spiral case cushion and the damage mode and evolution of the surrounding concrete have always been the research focus in this field. The SCS and surrounding concrete are the main supports to ensure the safe and stable operation of a hydropower station.

In recent years, scholars in China and elsewhere have conducted many studies on the embedding method of the SCS, achieving remarkable results. Qin et al. [5] conducted a collaborative stress model test on the volute and adjacent concrete structures of the Ertan Hydropower Station and found that pressure-maintaining pouring can mitigate the impact of internal hydraulic pressure (IWP) on the adjacent reinforced concrete. Ma et al. [6] demonstrated the embedding method of giant SCSs with high HD values and found that the cushion can significantly reduce the tensile stress of surrounding concrete as well as the magnitude of hydraulic pressure borne by the steel lining. Zhang et al. [7]

analyzed the stress and deformation characteristics of the SCS embedded using three different methods. They found that the cancellation of expansion joints and thrust rings in the cushion scheme has a negligible effect on the stress condition of the volute. As the optimization of the cushion scheme over time, scholars have proposed many safe and cost-effective embedding schemes, which have been widely used in different SCSs. Some scholars have studied the factors that influence the collective load-bearing capacity of the volute and adjacent concrete structures. For example, based on the contact relationship between the volute and the cushion, an analysis and comparison were conducted by Shen et al. [8], verifying the rationality of the contact element. By means of the three-dimensional nonlinear finite element method, Fu et al. [9] studied the influence of the elastic modulus, thickness, and laying range of the volute cushion on the bearing capacity of a hydropower station. Li et al. [10] utilized contact elements to simulate characteristics of frictional contact between the steel lining and the adjacent concrete, and the results indicated that the IWP could lead to deterioration in the adjacent concrete, and this deterioration may escalate with the repetitive impact of water pressure. Xu et al. [11,12] examined the sliding contact properties of the steel volute and the adjacent concrete when simulating the cushioned spiral case of large hydropower stations, providing a solid theoretical foundation for the construction of sizable hydropower stations. Wei et al. [13] introduced a new material interface contact element model, revealed the mechanical laws of the water-filled pressure-maintaining composite SCS, and verified the rationality of the contact element model. Zhang et al. [14] analyzed the nonlinear frictional contact between the steel lining and the concrete and found that the steel lining may experience relative sliding against the inner surface of the concrete due to the influence of internal water. Su et al. [15] investigated the impact of gap size and distribution on the pipe bearing capacity. They concluded that the load causing pipe cracking exhibits a linear relationship with the gap value, with the gap amount near the initial cracking site exerting control. In a related study, Fu et al. [16] analyzed the holistic structure of a hydropower station. They determined the maximum stress in different directions and pinpointed the location of maximum stress within the hydropower station structure. Ma et al. [17] examined the deformation characteristics of the surrounding rock within a subterranean powerhouse and found that the surrounding rock remains stable with low stress and deformation. Elastic cushions have been widely used in water conservancy projects to prevent the spiral case's IWP from being transmitted to the outer concrete and fully leverage the bearing capacity of the metal spiral case. However, the studies mentioned above rarely consider the impact of the cushion laying range on the stability of the SCS.

There are many studies on the damage and cracks in the concrete surrounding the SCS under different embedding methods. Wu et al. [18] analyzed the structure of a power station on the right bank of Three Gorges using the reinforced concrete elastic-plastic fracture damage model and obtained the damage range, crack width, and structural displacement of the concrete. Zhang [19] analyzed the damage to concrete surrounding the SCS and the flexibility of the stay ring based on the tensile softening characteristics of concrete and found that local damage usually appears in the peripheral weak areas, but the damage is too minor to cause significant destruction. Ma et al. [20] analyzed the water-filling pressure-maintaining pouring of surrounding concrete, unloading-caused gap, and water refilling for the spiral case of hydropower stations and concluded that the unevenness and premature closure of the gap between the steel lining and concrete increase the stress and damage to the concrete structure. The reliability of the cushion-spiral case joint bearing capacity is crucial to the safety and stability of the project. Some scholars have conducted a lot of research on the cushion-spiral case joint bearing performance and damage evolution. Li et al. [21] proposed a new numerical calculation method for vibration damage to concrete around the spiral case caused by water flow in the turbine channel based on the fluid–solid coupling theory. Hao et al. [22] performed a three-dimensional numerical simulation analysis of the SCS embedded using different methods. They found that the direct burial–cushion combination can effectively control concrete cracking in key

parts, significantly reduce concrete damage, prevent the uneven rise of the characteristic section of the generator pedestal (GP), and decrease the unbalanced thrust of the stay ring. Wu et al. [23] analyzed the stress and strength of thin-walled structures based on the surrounding thin-walled concrete of hydraulic turbines. Cui et al. [24] explored the mechanical laws under the joint load of a high-HD spiral case and peripheral structures. The results showed that most of the water-filled surrounding concrete is in the compressive stress state and is detached from the spiral case by about 3%. Mi et al. [25] analyzed the bearing capacity of the semi-cushioned spiral case based on the friction contact between the steel lining and the surrounding concrete and the bond–slip between the steel bars and concrete. They found that under the action of hydrostatic pressure, local damage in weak areas of the surrounding concrete may not cause structural failure due to insufficient strength. Xia et al. [26] optimized the elastic cushion of the turbine’s spiral case in the Fengman Hydropower Station and improved the concrete stress and deformation around the turbine’s spiral case to prevent concrete cracking. Given the preheating expansion characteristics of steel spiral cases, Gao et al. [27] proposed the preheating expansion method to embed the spiral case in hydropower stations. They found that the preheating expansion of steel spiral cases can be substituted by water-filled pressure-maintaining to some extent. Aikaterini S et al. [28] performed a nonlinear finite element analysis of reinforced concrete joints under static and quasi-dynamic loads and studied their failure modes from the perspectives of ultimate load and cracking mode. There are many studies on the impact of the spiral case embedding method on the surrounding concrete, but few studies on the optimization of the cushion for the SCS of high-HD hydropower stations and the damage mechanism of the surrounding concrete under extreme working conditions.

Scholars have conducted little research on the coupling relationship between the uneven lifting of the GP and concrete damage and the shear performance of the stay ring under the action of water. Given this, we adopted the concrete damaged plasticity (CDP) model to study the SCS of a large hydropower station on a river in southwest China. Considering the joint bearing capacity of the cushion and the spiral case, this article analyzed the impact of the cushion range on the load-bearing state of the SCS under the action of internal water, discussed the effect of the nonlinear factors of concrete materials on the stress deformation of the SCS and on the plasticity and damage cracking process of concrete, and explored the damage evolution rules of the SCS under extreme working conditions, providing a reference and theoretical support for further research on the failure mechanism and damage of cushioned spiral cases.

2. Methods and Related Theories

The objective of this paper was to investigate the impact of varying bedding areas on the distribution of damage in a concrete foundation and elucidate the failure mechanism and damage mode of a cushioned spiral case under increasing water load. The study employs the continuum damage plasticity (CDP) model, originally proposed by Lubliner et al. [29] and further developed by Lee and Fenves [30]. This theoretical framework is designed to address diverse damage states, incorporating two key damage variables—tensile damage and compressive damage—alongside a yield function featuring multiple hard variables. The uniaxial strength function is systematically decomposed into two integral components, specifically aligned with effective stress and elastic stiffness degradation. Notably, this approach skillfully decouples the elastoplastic response from the degradation damage response. Such decoupling proves instrumental in facilitating the numerical implementation of the model, enhancing its computational efficiency and effectiveness in simulating complex structural behaviors. Following the incremental theory of plasticity within the CDP model, the combined strain tensor ε consists of both the elastic strain ε^{el} and the equivalent plastic strain ε^{pl} .

$$\varepsilon = \varepsilon^{el} + \varepsilon^{pl} \quad (1)$$

When the damage to concrete approaches zero under a load, its stress–strain relationship is as follows:

$$\sigma = D^{el}(\varepsilon - \varepsilon^{pl}) \tag{2}$$

where σ represents the total stress, and D^{el} represents the elastic stiffness matrix.

When concrete is subjected to loading and undergoes damage, the stiffness degrades. Introducing the material’s damage factor as a parameter for characterization, the stress–strain relationship of concrete under these conditions becomes:

$$\sigma = (1 - d)\sigma = (1 - d)(\varepsilon - \varepsilon^p)E_0 \tag{3}$$

Under the cyclic and alternating application of loads, the early cracking and merging phenomena of concrete, as well as the interactions during the variation process, depend on the damage mechanism of the concrete. When the direction of the applied load changes, and a locally tensile area becomes compressive, the position will experience local recovery, known as a unilateral effect. Introducing the damage variable d under alternating loads, as well as the tensile and compressive damage variables d_t and d_c , the relationship among them is:

$$(1 - d) = (1 - s_t d_c)(1 - s_c d_t), \quad 0 \leq s_t, s_c \leq 1 \tag{4}$$

In the formula, s_t and s_c is the stiffness recovery stress.

$$\begin{cases} s_t = 1 - w_t r^*(\bar{\sigma}), 0 \leq w_t \leq 1 \\ s_c = 1 - w_c (1 - r^*(\bar{\sigma})), 0 \leq w_c \leq 1 \end{cases} \tag{5}$$

In the formula, $r^*(\bar{\sigma})$ is the weight factor associated with the principal stress in a multiaxial state. Among them:

$$r^*(\bar{\sigma}) \stackrel{\text{def}}{=} \frac{\sum_{i=1}^3 \langle \bar{\sigma}_i \rangle}{\sum_{i=1}^3 |\bar{\sigma}_i|}, \quad 0 \leq r^*(\bar{\sigma}) \leq 1 \tag{6}$$

In the formula, w_t and w_c is the stiffness recovery weight factor, which is related to the material properties; $\bar{\sigma}_i (i = 1, 2, 3)$ is the main stress component; $\langle x \rangle = (|x| + x)/2$.

The weight factor under uniaxial alternating load $w_c = 1$ (tension to compression), $w_t = 0$ (compression to tension). Figure 1 displays the stiffness recovery curve of the concrete damage model (CDP).

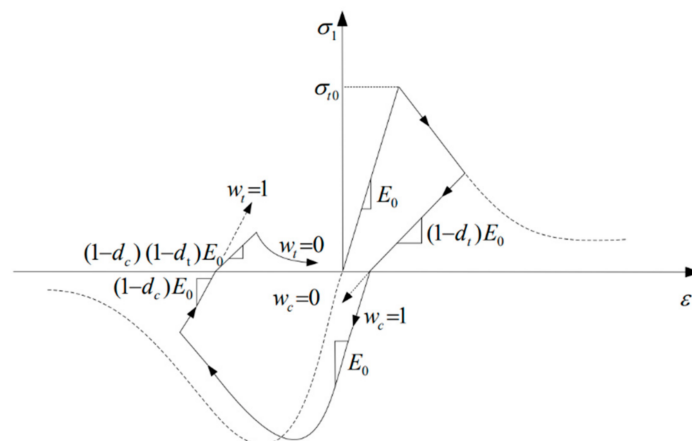


Figure 1. Stress–strain relation.

3. The Structural Model and Parameters of the Spiral Case

3.1. The Spiral Case Structural Model

The spiral case model was established based on a large hydropower station on a river in southwest China (Figure 2). The generator set section was 38 m long and 30.6 m wide from upstream to downstream. The upper end of the spiral case's structural model took the top of the GP, with an elevation of 582.35 m, the lower end took the right cone section of the draft pipe, and the outer end took the joint of the generator set section. The entire model was 27.95 m high. The structure mainly bore its dead weight, the IWP from the spiral case (3.43 MPa), the turbine layer load (50 kN/m²), the other floor load (30 kN/m²), the stator foundation plate (SFP) load, the lower frame load, and the crowd load. The model adopted full constraints at the bottom, normal constraints in the left and right bank directions, and spring constraints in the upstream and downstream directions, based on which the structure was analyzed and calculated.

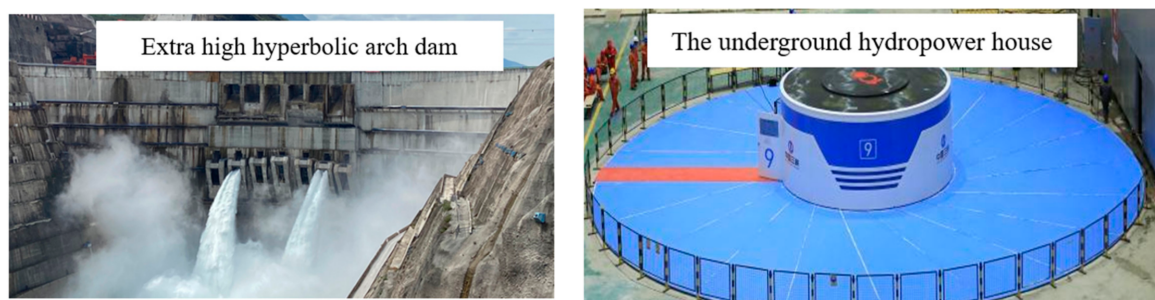


Figure 2. Real-time photos of the scene.

Major commercial software packages, ANSYS 19.0 and ABAQUS 6.14, were used to model and analyze the structure. The model consisted of 112,393 units and 110,903 joints. The steel spiral case and the stay ring adopted shell elements (Shell 181 Elements); the elastic cushion and the concrete around the spiral case adopted hexahedral solid elements (Solid 65 Elements); the beams and columns in the spiral case layer and the middle layer were simulated by beam elements (Beam 188 Elements), and the floor was simulated by shell elements (Shell 181 Elements). The periphery of the spiral case was made of C30 concrete with the plastic damage constitutive characterization based on the classic Lee–Fenves theory.

Figure 3 shows the finite element mesh of the spiral case model. The coordinate origin was set at the erection elevation axis of the turbine. The x-axis was the longitudinal direction of the powerhouse, with the direction from the right bank to the left bank as positive. The y-axis was the transverse direction of the powerhouse, with the direction from the downstream to the upstream as positive. The z-axis was the vertical direction of the powerhouse, with the upward direction as positive.

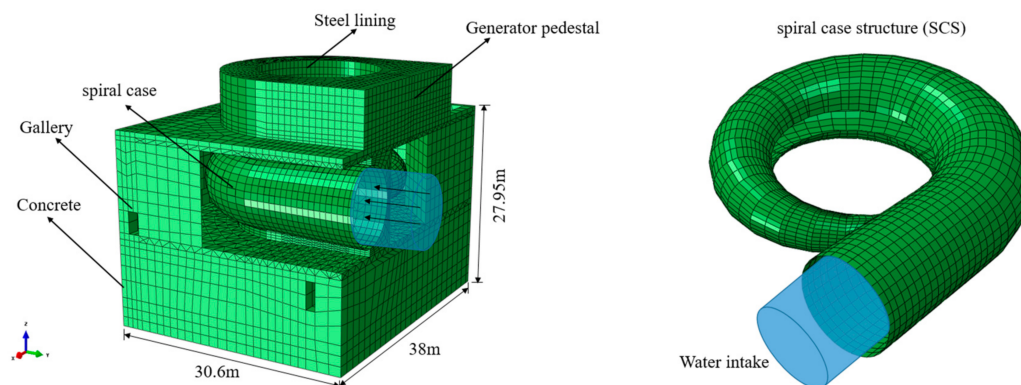


Figure 3. The overall model of the composite cushion-spiral case structure.

3.2. Load and Boundary Conditions

The loads encompassed the structural self-weight, the instantaneous water pressure (IWP) of 3.43 MPa jointly borne by the steel spiral case and concrete, as well as the loads exerted by the spiral case foundation plate (SFP) and lower bracket foundation plate (LBFP). In the nonlinear calculations, the application of loads not related to water loads preceded, in sequence, the installation of the spiral case and the pouring of concrete. Subsequently, the water pressure within the spiral case was applied. To account for the contact slip between the steel spiral case and the surrounding medium, a “surface-to-surface” contact element with a friction coefficient of 0.25 was established between the steel spiral case and the adjacent concrete and cushion. A boundary normal spring was set up between the upstream and downstream concrete of the generator set section and the surrounding rock, and an axial spring was set up at the upstream end of the spiral case’s straight pipe section. The bottom boundary of the model was confined. Some material parameters are shown in Table 1 below.

Table 1. Material parameters.

Material	Elastic Modulus E/MPa	Density/kg/m ^{−3}	Poisson’s Ratio
Concrete	2.8×10^4	2500	0.167
Spiral case	1.9×10^5	7850	0.235
Cushion	2.00	260	0.05
Stay ring	2.06×10^5	7850	0.29

Two calculation conditions were drawn up in this study: cushion wrap angle scheme and overload scheme. In the first scheme, the wrap angle increased from 0° to 270°, and the direct burial of the spiral case as well as the joint bearing capacity of the spiral case and the cushion were taken into account. In the second scheme, the overload increased from 1.0 to 2.0, and the impact of the cushion wrap angle on the spiral case and its surrounding concrete was analyzed. The above nine calculation schemes were used to fit the structural strength, stay ring shear strength, and generator pedestal lifting changes under loads in studying the spiral case-cushion, aimed at providing a theoretical reference for research on the evolution rules of structural damage.

4. Analysis of Uneven Lifting of the GP

4.1. Actual Measurement Comparison

During the operation, the water-turbine generator set will inevitably vibrate. The generator pedestal structure is the main support of the generator set, and its stiffness has an important influence on the stable operation of the latter. The generator pedestal structure mainly bears the static and dynamic loads of the generator set. Given its complex system and multiple openings, there are high requirements for the stiffness of the GP structure [30].

When the rotating parts of the generator set are installed, the spiral case, as the foundation of the GP structure, generally contains no water. However, its uneven upward displacement after water filling may cause the misalignment of rotating and fixed parts of the generator set, thereby affecting its stable operation. Therefore, special attention should be paid to the impact of the cushioned spiral case arrangement and the application of loads on the safe and stable operation of the generator set.

Figure 4 illustrates the positions of the eight monitoring points, while Figure 5 presents the comparison results. The computed outcomes closely resemble the monitored results, establishing the reliability of the calculations in this article. Thus, these calculations can furnish a theoretical foundation for the practical implementation of the project.

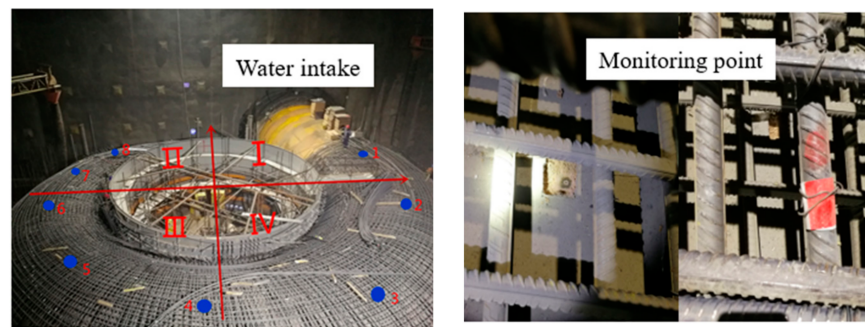


Figure 4. Real-time photos of on-site monitoring points. (I–IV is the first to fourth quadrants, and 1–8 is the eight monitoring points distributed in the above four quadrants.).

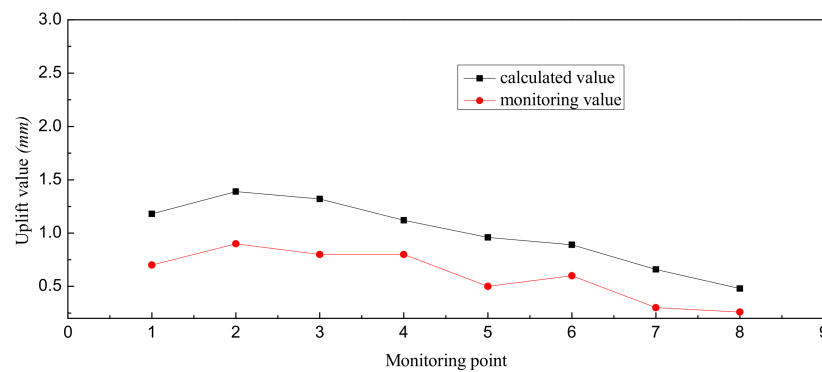


Figure 5. Comparison between calculated and monitored values.

4.2. Analysis of Uneven Lifting of the GP

As shown in Figure 6, 20 feature points (D1–D20) were set at the SFP, and 12 feature points (X1–X12) were set at the LBFP to explore the uplift rules of the GP before and after the action of internal water. Two calculation conditions were drawn up in this study. One of them was the overload scheme. In this scheme, the impact of the cushion wrap angle on the spiral case and its surrounding concrete was analyzed when the overload increased from 1.1 to 2.0. The other was the cushion wrap angle scheme. In this scheme, the wrap angle increased from 0° to 270°, and the effects of the spiral case’s direct burial and the spiral case-cushion joint bearing capacity on concrete were taken into account.

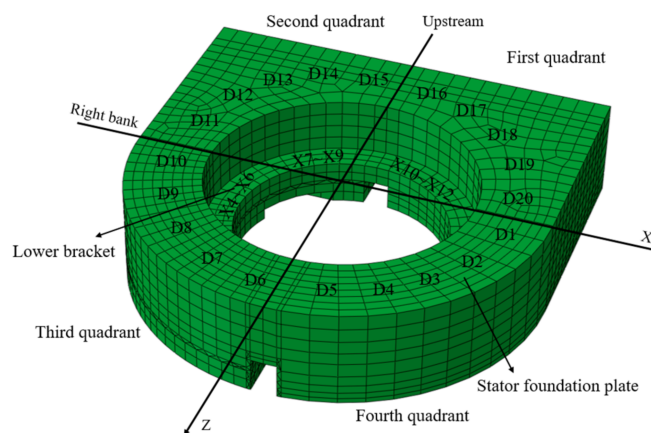


Figure 6. Schematic diagram of the stator foundation plate and lower bracket plate.

As shown in Figures 7 and 8, under the 1.0 overload, the SFP and the LBFP were lifted by only 1.18 mm and 1.26 mm, respectively, under the action of internal water, which was basically consistent with the actually measured generator pedestal displacement. The

displacement of the D16–D20 monitoring points at the SFP was more significant than that of other points, showing that the upward displacement of the GP mainly occurred in the inlet straight pipe section of the spiral case. The lifting of the LBFP was similar to the distribution of the SFP. If concrete damage and cracking were considered, the uneven deformation of the GP was significantly larger than the linear elastic calculation results.

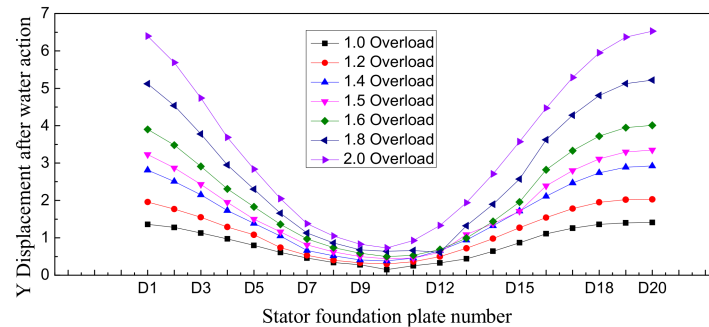


Figure 7. Displacement difference before and after water action in the stator foundation plate under different loading multiples.

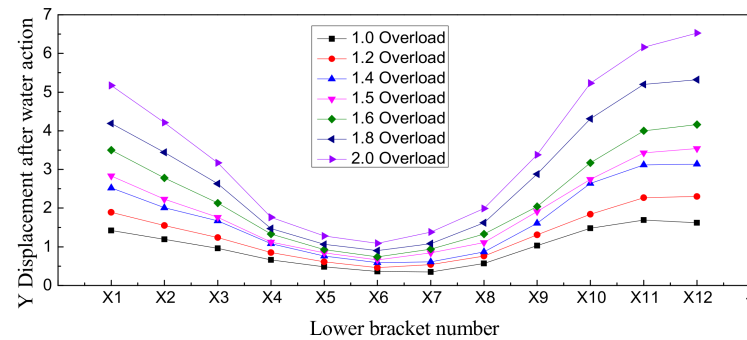


Figure 8. Displacement difference before and after water action in the lower bracket plate under different loading multiples.

As the load multiplied, the uneven lifting (the maximum vertical displacement difference between the foundation plates) of different SFPs increased linearly. This was also true for the uneven lifting of different LBFPs. In the case of 1.2 overload, the GP was lifted 1.73 mm at the inlet section of the spiral case. The uplift significantly increased when the overload rose to 1.4–2.0. This was consistent with the above-mentioned calculation result that the run-through damage mainly occurred in the case of 1.1–1.2 overload. As the overload increased, damage occurred to the concrete around the spiral case, ranging from the middle of the straight pipe section to the inlet section and extending downstream along the water flow, and the GP was lifted accordingly, showing that the concrete damage and cracking around the spiral case may cause the displacement of the GP. During this process, the lifting of the GP showed uniform linear growth. Within the range of 2.0 times the maximum design head, the GP did not deform greatly. It was found that the entire concrete structure of the spiral case has high crack resistance.

Figures 9 and 10 show the GP lifting changes in the SFP and LBFP with the cushion wrap angle variation. Under the same load, cushion shear modulus, and thickness, as the cushion wrap angle increased, the difference in the vertical displacement of the SFP and the LBFP before and after the action of water pressure in the spiral case decreased overall. This meant that increasing the cushion laying range could reduce the overall upward displacement of the GP. The uneven lifting (the maximum vertical displacement difference between the foundation plates) of different SFPs showed a decreasing trend. This was also true for the uneven lifting of different LBFPs. When the cushion wrap angle was less than 180°, the uneven lifting of the GP increased sharply as the wrap angle decreased. As shown

in the figure, the upward displacement of the GP in the 0° cushion scheme (namely, the direct burial scheme) increased to 4.94 mm, larger than that in the spiral case-cushion joint load-bearing scheme. A reasonable cushion-spiral case scheme could obviously reduce the upward displacement of the GP. The lifting amount of the GP under the cushion-spiral case joint load-bearing scheme was reduced by 74% compared with that under the direct burial scheme, indicating that the cushion setting can effectively control the uneven lifting of the GP. The upward displacement of the GP obtained in this study was consistent with the findings in the literature [31]. This was mainly because the cushion had a buffer effect. The cushion is a nonlinear material, and a reasonable cushion scheme can enhance the utilization of steel, reduce the stress concentration on the steel lining at the stay ring, and improve the stress of the concrete weak area around the end of the cushion.

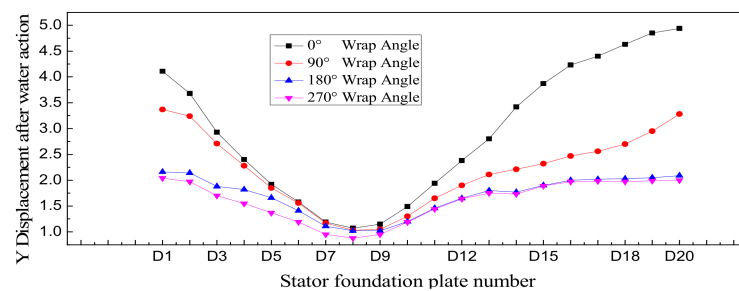


Figure 9. Displacement difference before and after water action in stator foundation plate under different cushion schemes.

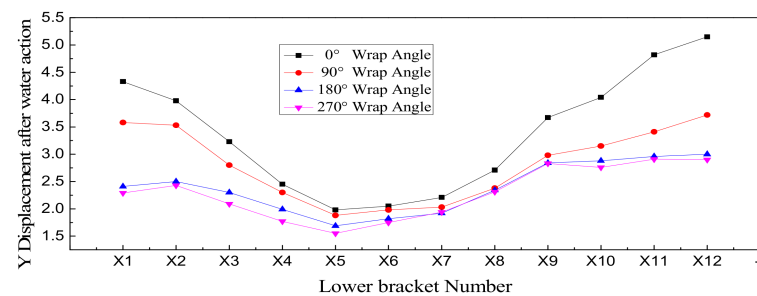


Figure 10. Displacement difference before and after water action in the lower bracket plate under different cushion schemes.

5. Effect of Unbalanced Water Thrust on the Stay Ring

The steel spiral case of hydropower stations is a semi-enclosed spiral structure that is not completely axially symmetrical and has an inner opening. During the operation of the generator set, the resultant force of the IWP acting on the steel spiral case is not zero, and a large axial water thrust pointing downstream will be generated at the inlet, which is determined by multiplying the cross-sectional area of the inlet by the IWP. Meanwhile, the water thrust will generate torque relative to the central vertical axis of the generator set. Due to the asymmetrical shape and stiffness of the spiral case, the steel spiral case also bears horizontal radial unbalanced forces [32]. The study [33] was the first to reveal that the spiral case's stay ring is one of the main parts bearing unbalanced water thrust and preliminarily discussed the impact of expansion joints, thrust rings, and cushion laying on the bearing capacity of the stay ring. The study [34] further explored the damage and cracking characteristics of concrete around the spiral case, and the results showed that concrete cracking or damage has a significant impact on the flexibility of the stay ring.

The unbalanced force borne by the stay ring is transmitted to the concrete mainly through the friction between the anchor bolts, ring plates, and concrete. If the unbalanced force is too large, it may damage the connection between the upper and lower ring plates and the concrete, threatening the strength of the anchor bolts, which is extremely detrimental to the stable operation of the generator set [21]. Among the schemes proposed in

this article, the first four mainly concerned the influence of the cushion wrap angle on the shear force, and the last five concerned the limit conditions of overload and changes in the shear force.

Table 2 gives the value of the shear force in all directions in each scheme. The comparison of the first four schemes showed that when the cushion wrap angle β was in the range of 0° – 90° , the absolute value of F_x increased rapidly with the increase in the cushion wrap angle (along the x direction), while the absolute value of F_z decreased rapidly. When the cushion wrap angle was 90° , F_x reached the maximum, namely 13.46 MN, and F_z reached the minimum, about 1.11 MN. When the cushion wrap angle exceeded 90° , the absolute value of F_x decreased rapidly, while the absolute value of F_z increased rapidly. When the cushion wrap angle reached 200° , F_x was almost reduced to zero and then increased in the opposite direction. When the cushion wrap angle was 270° , F_x reached the maximum in the negative direction, namely -6.20 MN. The absolute value of F_z reached the maximum when the cushion wrap angle was 180° , and then decreased in the opposite direction. When the cushion wrap angle was 270° , F_z was reduced to 4.45 MN.

Table 2. Calculation results of the shear forces for each scheme.

Overload	Wrap Angle	F _x	F _z	F
1.0	0°	5.07	−13.05	14.00
1.0	90°	13.46	1.11	13.51
1.0	180°	7.74	14.53	16.46
1.0	270°	−6.20	4.45	4.65
1.2	270°	−10.63	7.07	12.77
1.4	270°	−14.66	9.05	17.22
1.6	270°	−18.19	9.23	20.39
1.8	270°	−20.92	9.52	22.98
2.0	270°	−22.57	9.61	24.53

Figure 11 shows the value and direction of each resultant shear force. As shown in the figure, the horizontal shear force F on the stay ring first increased and then decreased as β increased. F reached the maximum when β was 180° , namely 16.46 MN, and then decreased as the cushion wrap angle increased. When the cushion wrap angle was 270° , the resultant force reached the minimum of the absolute value, only 4.65 MN. At this time, the resultant shear force on the stay ring was also the minimum. This indicated that the resultant shear force of the stay ring rotates in the clockwise direction (water flow direction) as the cushion wrap angle increases, affecting the value of the shear force.

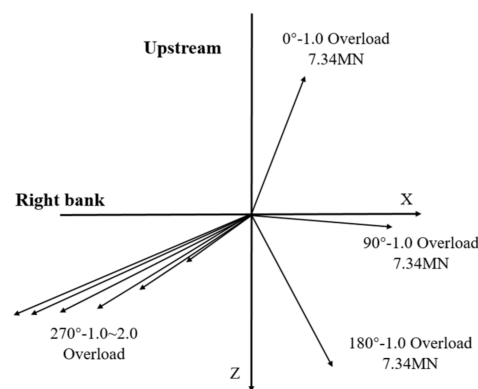


Figure 11. Relationship between variations in the shear vector in the stay ring.

As shown in the third quadrant of Figure 11 and Table 2, the last five schemes that changed with the overload multiple had little effect on the direction of shear forces. Almost all the shear forces pointed to the downstream right bank (facing downstream is deemed as

the positive direction). Numerically, both F_x and F_z showed linear growth according to load changes, and the resultant shear force reached the maximum of 24.53 MN at 2.0 overload. Given that the stay ring bears unbalanced forces, a reasonable cushion scheme can help reduce the stress concentration on the steel lining at the stay ring and increase the stay ring's shear resistance and the SCS's stability.

6. Analysis of Damage Evolution Rules

For the SCS with a high HD value (the product of the designed IWP and the inlet diameter of the steel spiral case) selected in this study, the concrete damage evolution process under the spiral case-cushion joint load-bearing scheme is particularly important due to its high head. Overloads of 1.1, 1.5 and 2.0 times the head were selected to calculate and analyze the said process.

Figure 12 shows several typical stress distributions of steel bars at different locations under the IWP overload. It was found that the large steel stress basically appeared in the areas where concrete damage was serious, which was consistent with the distribution of the damage zone. In the case of 1.1 overload, the maximum stress of the three layers of circumferential steel bars around the spiral case was between 90 MPa and 110 MPa, meeting the concrete crack width requirements for the nonlinear calculation and analysis. In the case of 1.2 overload, the maximum stress of the three layers of circumferential steel bars was within 130–170 MPa. The maximum IWP that met the crack width requirements of the SCS was 1.1–1.2 times the maximum design head.

Figure 13 shows the damage evolution of the overall external structure of the concrete around the spiral case under the IWP overload. The concrete damage near the nasal end extended to the upstream side along the inner waistline of the straight pipe section. Slight damage occurred at the upstream end at 1.1 times the maximum design head. As the overload increased, the damage extended further from the left side to the right side of the generator set and exceeded the plane where the center line of the generator set was located at 1.2 times the maximum design head. The damage zone in the intersection between the GP at the top of the spiral case and the turbine floor gradually extended to the right side of the generator set along the intersection line and then to the 180° meridian plane.

As the head increased to 1.4 times the overload head, a run-through damage zone appeared at the downstream end of the left straight pipe section. The damage zone along the intersection between the GP at the top of the spiral case and the turbine floor gradually expanded to the flow channel as the overload head increased and finally appeared through the straight pipe section. When the internal pressure increased to 1.2 overload, damage appeared inside the thinnest part of the concrete around the spiral case in the lower left of the straight pipe section. When the internal pressure increased to 1.6 overload, damage expanded to the outermost side. The concrete at the top of the manhole on the downstream side of the GP was slightly damaged during the overloading process. At 1.6 times the head, the damage zone extended from the upper rim of the stay ring to the bottom plate of the manhole. At the outer waistline of the concrete surrounding the spiral case, a damage zone appeared at the entrance of the straight pipe section in the case of 1.8 times the head.

Figure 14 shows the damage evolution of the overall internal structure of the concrete around the spiral case under the IWP overload. As shown in the figure, the concrete inside the upper flow channel was slightly damaged under the maximum design head. As the IWP increased to 1.2 times the design head, the damage extended from the middle of the straight pipe section to the inlet section and then expanded downstream along the water flow and to the outside of the concrete around the spiral case along the 135° direction in the meridian plane. The concrete stress around the spiral case was mainly tensile stress, and some of it was compressive stress. The tensile stress became larger from inside to outside and was the largest at the top of the spiral case, where the concrete was the thinnest. The tensile stress also concentrated on the straight pipe section of the spiral case, near the nasal end, where the steel lining was the largest in diameter and the concrete was the thinnest. Damage easily occurred here and became less from outside to inside.

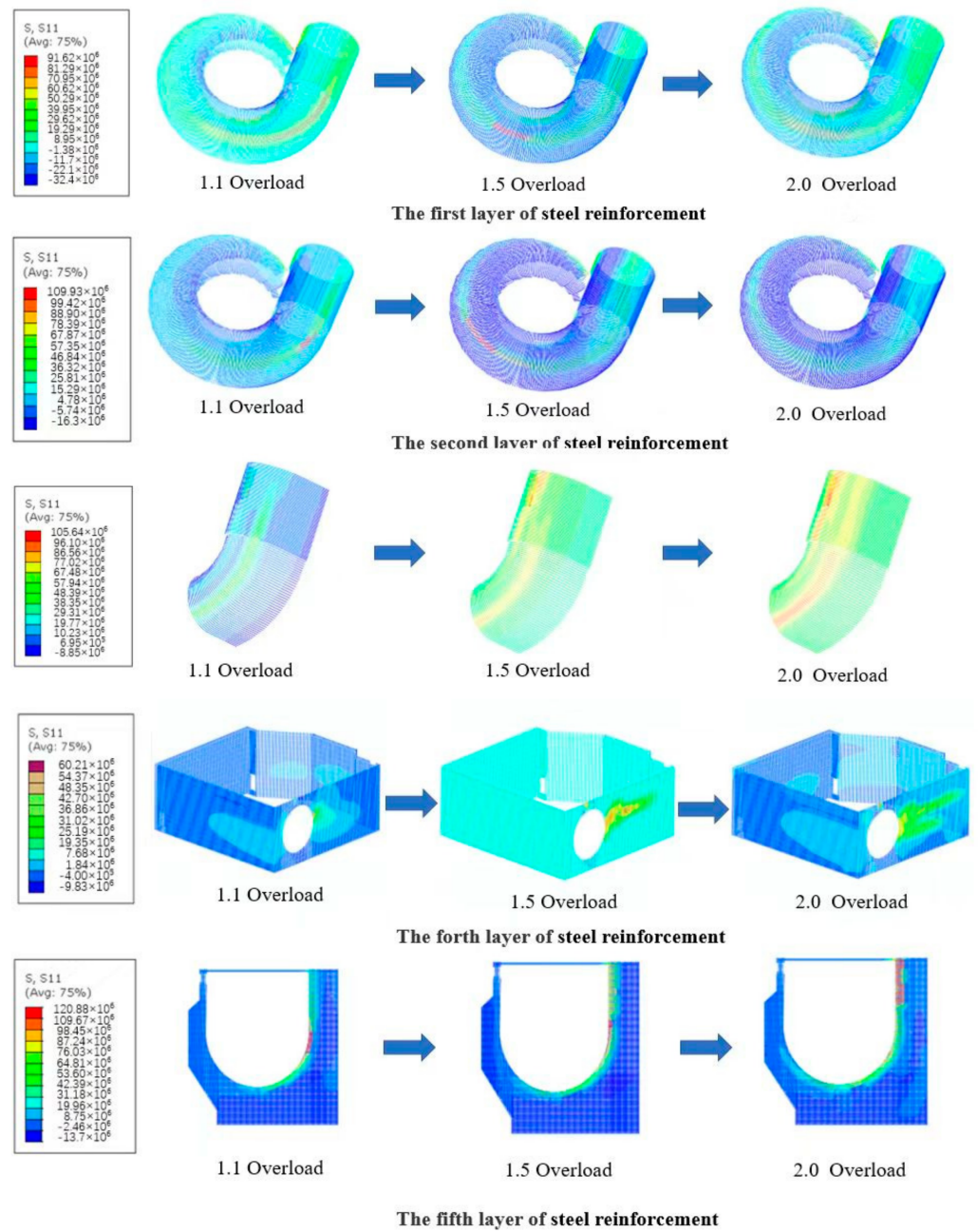


Figure 12. Stress distribution diagram of steel bars.

Overall, as the IWP increased, the plastic damage area of the concrete around the spiral case gradually expanded. When the IWP increased to 1.1–1.2 times the head, run-through cracks were easily formed.

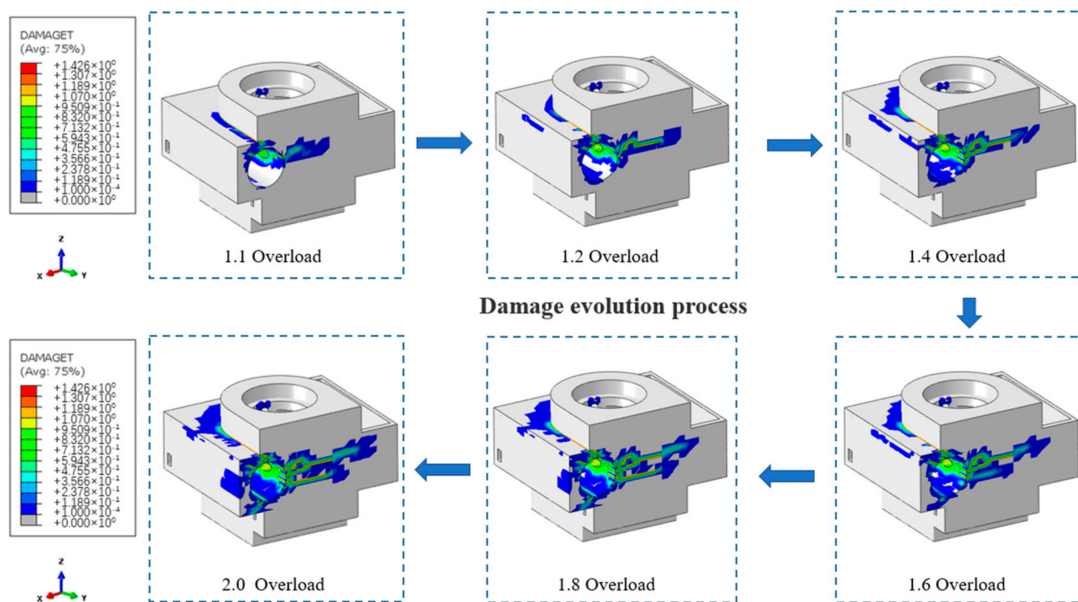


Figure 13. Development diagram of damage to the overall structure of concrete around the spiral case under internal water pressure overload.

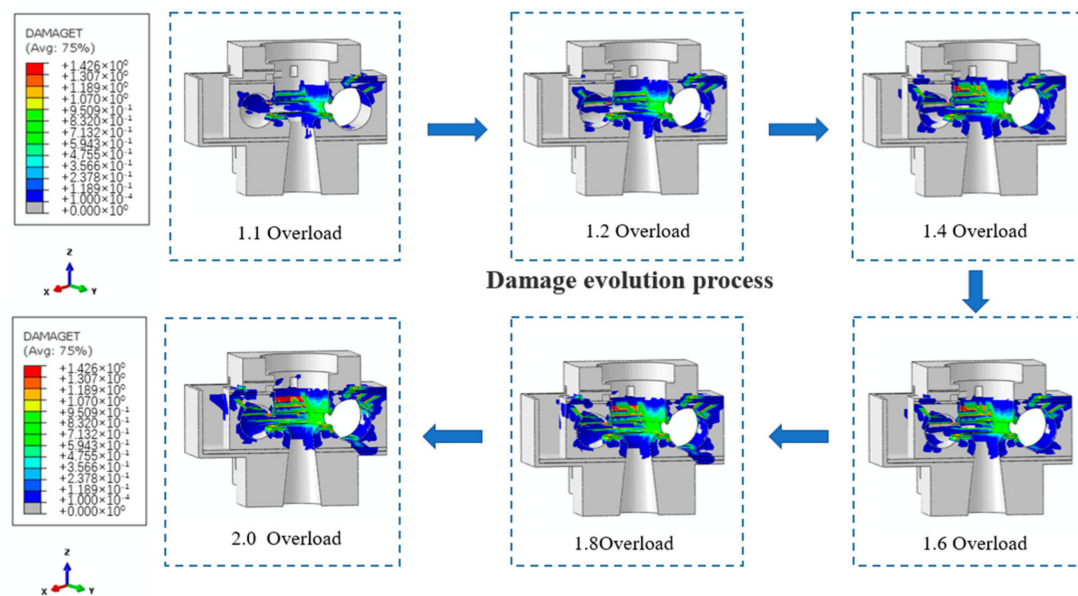


Figure 14. Development of damage to the overall structure of concrete around the spiral case under internal water pressure overload.

In summary, the cushion scheme can make the role of the “cushion-spiral case” joint bearing system better leveraged than the direct burial scheme and the water-filled pressure-maintaining scheme. However, the above studies are limited to a small-time scale, fail to consider the long-term creep and durability of the cushion material, and lack insight into the cushion performance degradation and failure mechanism during the long-term operation of the generator set. The impact of the cushion material on the stable operation of the generator set during its service life is still unclear. Further research on the performance evolution of the cushion material on a larger time scale is necessary, to reveal the mechanical properties of the cushion throughout its life cycle.

7. Conclusions

In this study, we established a spiral case-cushion joint load-bearing model to analyze the impact of the cushion range on the bearing capacity of the SCS under the action of internal water and explore the damage mechanism of the concrete structure around the spiral case under the limit states. The conclusions drawn are as follows:

(1) As the IWP increases, the plastic damage area of the concrete around the spiral case gradually expands. When the IWP rises to 1.1–1.2 times the head, a run-through crack is easily formed. For the SCS with a high HD value, a reasonable cushion scheme can significantly reduce the damage level of the surrounding concrete, and a scheme with a large wrap angle can facilitate the joint load-bearing function of the structure and ensure the integrity of the surrounding concrete.

(2) The upward displacement of the GP mainly occurs in the straight pipe section at the inlet of the spiral case. The lifting of the LBFP is similar to the distribution of the SFP. As the load multiplies, the uneven lifting (the maximum vertical displacement difference between the foundation plates) of different SFPs increases linearly. Damage and cracking of the concrete around the spiral case may cause the displacement of the GP.

(3) As the cushion wrap angle increases, the difference in the vertical displacement of the SFP and the LBFP before and after the action of water pressure in the spiral case decreases overall. The lifting amount of the GP under the cushion-spiral case joint load-bearing scheme is reduced by 74% compared with that under the direct burial scheme, indicating that the cushion setting can effectively control the uneven lifting of the GP.

(4) The resultant shear force of the stay ring rotates in the clockwise direction (water flow direction) as the cushion wrap angle increases, affecting the value of the shear force. Changes in the overload multiple have little effect on the direction of the shear force, which points to the downstream right bank (facing downstream is deemed as the positive direction). Numerically, both F_x and F_z show linear growth according to load changes. Given that the stay ring bears unbalanced forces, a reasonable cushion scheme can help increase the stay ring's shear resistance and the SCS's stability. This paper can serve as a theoretical basis and reference for optimizing cushioned SCSs, enhancing shear resistance, and controlling the lifting of the GP to ensure the safe and stable operation of generator sets.

(5) Compared with existing research, this study proves that the cushion structure plays a positive role between the spiral case and the surrounding concrete, but it cares less about the long-term creep and durability of the cushion material and the material performance degradation and failure mechanisms during the operation of the generator set. Further research needs to be conducted on the types and characteristics of cushion materials and the evolution mechanism of the structure under long-term operating conditions.

Author Contributions: Conceptualization, G.W. and W.X.; methodology, W.X.; software, W.X.; validation, Z.M.; formal analysis, W.X.; investigation, G.W.; resources, F.K.; data curation, G.W.; writing—original draft preparation, W.X.; writing—review and editing, W.X.; visualization, W.X.; supervision, G.W.; project administration, W.X.; funding acquisition, W.X. All authors have read and agreed to the published version of the manuscript.

Funding: This work was supported by the National Natural Science Foundation of China 464 (51979027, 52079022).

Institutional Review Board Statement: Not applicable.

Informed Consent Statement: Not applicable.

Data Availability Statement: Data are contained within the article.

Conflicts of Interest: The authors declare no conflicts of interest.

References

1. Zhang, Z.M.; Wu, H.G.; Shi, C.; Zhang, Q.-L.; Su, K.; Hu, L. Numerical modeling of preloaded filling spiral case structure. *Lat. Am. J. Solids Struct.* **2018**, *15*, 1–19. [[CrossRef](#)]

2. Denisova, S.E.; Denisova, M.V. Analysis of hydropower potential and the prospects of developing hydropower engineering in south ural of Russian federation. *Procedia Eng.* **2017**, *206*, 881–885. [[CrossRef](#)]
3. Behal, G. Hydropower generation overcoming system limitations. *IEEE Power Energy Mag.* **2020**, *18*, 106–108. [[CrossRef](#)]
4. Wu, H.; Gao, X.; Fu, D. Review and prospect in research and application of spiral case structure in hydropower plant. *J. Hydraul. Eng.* **2021**, *52*, 770–780.
5. Qin, J.Z.; Ma, S.D.; Wu, H.G.; Kuang, H.J. Experiment on material model of steel spiral case and surrounding reinforced concrete of Ertan Hydropower Station. *J. Hydraul. Eng.* **1999**, *6*, 11–15.
6. Ma, Z.Y.; Zhang, Y.L.; Chen, J.; Cheng, G.R.; Wang, Y. The Feasibility Evaluation of the Giant Spir al Case Using Cushion Layer. *J. Hydroelectr. Eng.* **2006**, *32*, 28–32.
7. Zhang, Y.L.; Ma, Z.Y.; Cheng, G.R.; Chen, J. Strength and stiffness analysis of spiral casing with different embedded manners. *J. Hydraul. Eng.* **2006**, *37*, 1206–1211.
8. Shen, Y.; Wu, H.G.; Jiang, K.C. Analysis of contact on spiral case with cushion layers of large hydropower station. *J. Hydraul. Eng.* **2006**, *25*, 74–78.
9. Fu, H.X.; Ma, Z.Y.; Dong, Y.X. Study on structure of cushion layer for spiral case in hydropower station. *J. Hydraul. Eng.* **2003**, *2003*, 85–89.
10. Li, Z.; Li, X.Z. Three-Dimensional Damage Analysis of Concrete Surrounding the Spiral Case in the Nuozhadu Hydropower Station. *Adv. Mater. Res.* **2012**, *393–395*, 1048–1053. [[CrossRef](#)]
11. Xu, X.Y.; Kang, Y.B.; Zhang, D. Study on Optimization under Internal Water Pressure of Spiral Case of Hydropower Station. *Appl. Mech. Mater.* **2013**, *438–439*, 834–838. [[CrossRef](#)]
12. Zhang, J.W.; Zhang, Y.N.; Yuan, S.F. Study on friction coefficient of spiral case with cushion layer in large-scale hydropower plant. *Appl. Mech. Mater.* **2011**, *71–78*, 4248–4251. [[CrossRef](#)]
13. Wei, B.; Wang, F.; Xu, Z.K.; Jiang, Z.X. Nonlinear Contact Analysis on the Spiral Case Composite Structure in Pumped Storage Power Station. *J. Yangtze River Sci. Res. Inst.* **2015**, *32*, 109–118.
14. Zhang, Q.L.; Wu, H.G. Sliding behavior of Steel Liners on Surrounding Concrete in c-Cross-sections of Spiral Case Structures. *Struct. Eng. Int.* **2016**, *26*, 333–340. [[CrossRef](#)]
15. Su, K.; Yang, Z.J.; Wu, H.G.; Zhou, L.; Shi, C.Z. Influence of Gap on Bearing Mechanism of Steel-Lined Reinforced Concrete Penstock. *J. Tianjin Univ. (Sci. Technol.)* **2018**, *52*, 967–976.
16. Jian, F.; Tang, T.D.; Wen, X.L.; Guo, X.M.; Zhao, J.W. Analysis of bulb Turbine Hydropower Station plant with 3D Finite Element Method. *Adv. Mater. Res.* **2011**, *243*, 4539–4543.
17. Ma, S.; Huang, T.S.; Bao, X.; Wang, Z.; Zhang, H.; Liu, G. Deformation analysis of underground powerhouse of a large hydropower station based on FLAC3D. *IOP Conf. Ser. Earth Environ. Sci.* **2021**, *632*, 042033. [[CrossRef](#)]
18. Wu, H.G.; Jiang, K.C.; Shen, Y. Three-dimensional nonlinear finite element static calculation of complete bearing spiral case. *J. Hydraul. Eng.* **2006**, *37*, 1323–1328. (In Chinese)
19. Zhang, C.H. Static and Dynamic analysis of Large-Scale Hydropower House and Spiral Case Structure. Ph.D. Thesis, Dalian University of Technology, Dalian, China, 2010.
20. Ma, Z.Y.; He, P.C.; Zhang, Y.L.; Zhang, H.Z. Nonlinear simulation analysis for preloading spiral case of keeping constant internal water pressure of hydropower station. *J. Dalian Univ. Technol.* **2010**, *50*, 1014–1019.
21. Li, Z.; Zhang, X.Y.; Zhang, L.X. Research on vibration and damage mechanisms of spiral casing structure on large-scale hydraulic turbine based on FSI method. *Chin. J. Solid Mech.* **2014**, *35*, 18–26.
22. Hao, J.G.; Fu, D.; Wu, H.G. Nonlinear structure analysis of spiral case with combination scheme of direct embedment and cushion layer in Gongguoqiao hydropower station. *Eng. J. Wuhan Univ.* **2014**, *47*, 306–310.
23. Wu, J.; Zhang, Y.J.; Cheng, P.; Gao, L. Stress analysis on outside thin-wall concrete of spiral case in powerhouse of Dadinkowa Hydropower Station House. *Water Resour. Hydropower Eng.* **2017**, *48*, 50–55.
24. Cui, W.; Liu, N.T.; Zhu, Y.B.; Guo, Y.; Li, M.; An, G. Mechanical simulation analysis on joint load-bearing process of preload filling spiral case with its surrounding structure. *Water Resour. Hydropower Eng.* **2018**, *49*, 73–79.
25. Mi, S.Z.; Gao, C.B. Analysis on nonlinear joint bearing capacity of semi-cushion spiral case of large hydropower station. *Water Resour. Hydropower Eng.* **2019**, *50*, 101–107.
26. Xia, Z.Y.; Hu, Y.H.; Li, J.W.; Jia, W. Optimal analysis on elastic cushion for hydro-turbine spiral case in powerhouse of Fengman Hydropower Station. *Water Resour. Hydropower Eng.* **2020**, *51*, 106–110.
27. Gao, X.F.; Wu, H.G.; Yu, P.; Fu, D. Study on embedment method of spiral case based on thermal effect under preheating condition in hydropower station. *Huazhong Univ. Sci. Tech. (Nat. Sci. Ed.)* **2021**, *49*, 110–115.
28. Genikomsou, A.S.; Polak, M.A. Finite element analysis of punching shear of concrete slabs using damaged plasticity model in ABAQUS. *Eng. Struct.* **2015**, *98*, 38–48. [[CrossRef](#)]
29. Lubliner, J.; Oliver, J.; Oller, S.; Oñate, E. A Plastic-Damage Model for Concrete. *Int. J. Solids Struct.* **1989**, *25*, 299–326. [[CrossRef](#)]
30. Lee, J.; Fenves, G.L. Plastic-Damage model for cyclic loading concrete structures. *J. Eng. Mech.* **1998**, *124*, 892–900. [[CrossRef](#)]
31. Chen, J.; Jiang, L.W.; Ma, Z.Y. Effect of cushion layer on stiffness of generator pedestal and stay ring structure in hydropower station. *Water Resour. Power* **2012**, *30*, 65–69.
32. Qi, Y.F.; Chen, Q.; Gong, Y.Q.; Xie, Z.Q. Optimization analysis of giant spiral case with combined embedding method. *IOP Conf. Ser. Earth Environ. Sci.* **2019**, *304*, 032064. [[CrossRef](#)]

33. Zhang, H.Z.; Yao, S.X.; Ma, Z.Y.; Li, X.J. Analysis of shear property of stay rings for spiral case with cushion layer under unbalanced hydraulic thrust. *J. Dalian Univ. Technol.* **2013**, *53*, 565–571.
34. Yao, S.X.; Sun, C.H.; Wang, D.D. A preliminary study of unbalanced hydraulic thrust in the spiral case structure. *Northwest Hydropower* **2010**, *2010*, 16–20.

Disclaimer/Publisher’s Note: The statements, opinions and data contained in all publications are solely those of the individual author(s) and contributor(s) and not of MDPI and/or the editor(s). MDPI and/or the editor(s) disclaim responsibility for any injury to people or property resulting from any ideas, methods, instructions or products referred to in the content.